Fourth-order interference of joint single-photon wave packets in lossless optical systems

Richard A. Campos
Department of Applied Physics, Columbia Radiation Laboratory, Columbia University, New York, New York 10027

Bahaa E. A. Saleh
Department of Electrical and Computer Engineering, University of Wisconsin, Madison, Wisconsin 53706

Malvin C. Teich
Departments of Electrical Engineering and Applied Physics, Columbia Radiation Laboratory, Columbia University, New York, New York 10027

(Received 13 June 1990)

We examine the fourth-order interference properties of two photons at a lossless four-port optical device. The photon pair is represented by a joint single-photon wave-packet state with arbitrary spectral composition. We explicitly determine the coincidence probabilities at the output ports of a beam splitter and a Mach-Zehnder interferometer when the incident wave packet is described by a joint Gaussian spectral distribution and the two photons are incident one at each port of the device. For uncorrelated and distinguishable input photons, the fourth-order interference is readily understood in terms of the particle or wave behavior of each photon acting separately. On the other hand, highly correlated photon pairs, such as those generated from spontaneous parametric down-conversion, exhibit fourth-order interference effects at the output of the interferometer that depend expressly on the joint nature of the photon-pair wave packet, and cannot be described by the particle or wave behavior of either photon.

I. INTRODUCTION

The production of photon pairs from atomic cascade processes[1] and parametric down-conversion[2] has permitted a number of fundamental experiments to be carried out.[3–7] In particular, if both photons are incident at one of the ports of a beam splitter, each of them produces an ouput photon-number distribution consistent with the behavior of distinguishable *classical particles,*[5] whereas if both are directed to one input port of an interferometer, each of them generates a photon-number distribution exhibiting second-order interference effects akin to those of *classical waves* as the path-length difference in the device is altered.[3,7]

However, if the photons are direct to *both input ports* of these devices, the ouput photon-number distribution exhibits fourth-order interference effects that cannot be explained by either simple particle or wave behavior, as has been confirmed in beam-splitter experiments.[4,6] The precise behavior to be expected is sensitive to the spectral correlation of the photons, which reflects the degree to which they are entangled at the source. These effects can be observed by two photodetectors working in coincidence.

In this paper we consider the interference of two photons at an arbitrary lossless four-port optical device when each of them is incident on one of the input ports. In Sec. II we construct joint single-photon wave packets with an arbitrary degree of spectral correlation and employ this description in Sec. III to obtain the coincidence probabilities at the output of the device. We consider the lossless beam splitter as an illustrative example and recover a number of results that were previously obtained. We then apply the theory to the Mach-Zehnder interferometer and delineate a broad range of fourth-order interference effects. We discuss our principal results in Sec. IV.

II. PHOTON WAVE PACKETS

According to the quantum theory of optical coherence, the electromagnetic field can be expanded in modes having a single variety of polychromatic photons excited.[8] These wave-packet modes are constructed from weighed superpositions of the monochromatic modes of the field. For simplicity, we consider a field of known polarization, quantized in a one-dimensional cavity of infinite length. A wave-packet operator can be defined as[9]

$$\hat{A}^{\dagger}(\epsilon) \equiv \int_0^{\infty} \epsilon(\omega)\hat{a}^{\dagger}(\omega)d\omega \ , \tag{1}$$

where $\epsilon(\omega)$ is a complex amplitude, and $\hat{a}^{\dagger}(\omega)$ is the continuum raising operator at the angular frequency ω, obeying the commutator relation

$$[\hat{a}(\omega),\hat{a}^{\dagger}(\omega')] \equiv \hat{a}(\omega)\hat{a}^{\dagger}(\omega') - \hat{a}^{\dagger}(\omega')\hat{a}(\omega) = \delta(\omega-\omega')\hat{I} \ . \tag{2}$$

The symbol $\hat{I}$ denotes the identity operator ($\hat{I}\hat{O}=\hat{O}$, where $\hat{O}$ is an arbitrary operator), while $\delta(\omega-\omega')$ is the Dirac delta function. This wave-packet operator obeys the boson commutation relation

$$[\hat{A}(\epsilon), \hat{A}^{\dagger}(\epsilon)] = \hat{I} \ , \tag{3}$$

provided the amplitude $\epsilon(\omega)$ is normalized such that

$$\int_0^\infty |\epsilon(\omega)|^2 d\omega = 1 \ . \tag{4}$$

A single-photon wave-packet state is obtained by permitting the operator of Eq. (1) to act on the vacuum according to

$$|1;\epsilon\rangle \equiv \hat{A}^\dagger(\epsilon)|0\rangle = \int_0^\infty \epsilon(\omega)|1_\omega\rangle d\omega \ , \tag{5}$$

where $|1_\omega\rangle \equiv \hat{a}^\dagger(\omega)|0\rangle$ are the monochromatic single-photon states. The probability $P(\omega)d\omega$ of observing a photon of frequency between ω and $\omega+d\omega$ in this wave-packet state is

$$P(\omega)d\omega \equiv |\langle 1_\omega|1;\epsilon\rangle|^2 d\omega = |\epsilon(\omega)|^2 d\omega \ , \tag{6}$$

which integrates to unity via Eq. (4).

We now consider the coherence properties of single-photon wave packets. Since only one mode is excited, the positive-frequency part of the electric field (normalized to photon units) can be represented at time t by[8]

$$\hat{E}^{(+)}(t) \equiv (2\pi)^{-1/2} \int_0^\infty \hat{a}(\omega) e^{-i\omega t} d\omega \Longleftrightarrow V(t)\hat{A}(\epsilon) \ , \tag{7}$$

where the symbol $\Longleftrightarrow$ denotes an equivalence, and $V(t)$ is the temporal profile of the single-photon wave packet,

$$V(t) \equiv (2\pi)^{-1/2} \int_0^\infty \epsilon(\omega) e^{-i\omega t} d\omega \ . \tag{8}$$

From Eqs. (3), (5), and (7), the Glauber first-order correlation function of the positive-frequency part of the field $\hat{E}^{(+)}(t)$ at time t, with its adjoint $\hat{E}^{(-)}(t)$ at time $t+\tau$, can be written[10,11]

$$\begin{aligned} G^{(1)}(t,\tau) &\equiv \mathrm{Tr}[\hat{\rho}\hat{E}^{(-)}(t+\tau)\hat{E}^{(+)}(t)] \\ &= V^*(t+\tau)V(t) \ , \end{aligned} \tag{9}$$

where Tr denotes a trace over a density operator $\hat{\rho}$, which is given here by $\hat{\rho} = |1;\epsilon\rangle\langle 1;\epsilon|$.

A normalized average of this function within a time window long enough to capture the full wave packet (we represent the window as effectively infinite) follows from Eqs. (6)–(9),

$$\begin{aligned} \gamma(\tau) &\equiv \frac{\int_{-\infty}^\infty G^{(1)}(t,\tau)dt}{\int_{-\infty}^\infty G^{(1)}(t,0)dt} \\ &= \int_0^\infty P(\omega) e^{i\omega\tau} d\omega \ . \end{aligned} \tag{10}$$

$\gamma(\tau)$ is therefore the characteristic function of the probability density $P(\omega)$. The coherence time of a single-photon wave packet can then be defined according to[12]

$$t_c \equiv \pi^{-1/2} \int_{-\infty}^\infty |\gamma(\tau)|^2 d\tau \ . \tag{11}$$

As a particular example, we consider a single-photon wave packet described by the complex amplitude

$$\epsilon(\omega) = (2\pi\sigma^2)^{-1/4} \exp\left[-\left[\frac{\omega-\omega_0}{2\sigma} \right]^2 \right] \exp(-i\omega t_0) \ , \tag{12}$$

where ωt_0 is the phase associated with a time shift t_0. According to Eq. (6), it defines a Gaussian probability density with center frequency ω_0 and spectral width σ,

$$P(\omega) = (2\pi\sigma^2)^{-1/2} \exp\left[-\frac{(\omega-\omega_0)^2}{2\sigma^2} \right] \ . \tag{13}$$

For a narrow-band profile ($\sigma \ll \omega_0$), we find from Eqs. (10) and (11) that the normalized first-order correlation function is

$$\gamma(\tau) = \exp(-\sigma^2\tau^2/2)\exp(i\omega_0\tau) \ , \tag{14}$$

and the coherence time

$$t_c = \frac{1}{\sigma} \tag{15}$$

is just the inverse bandwidth of the photon wave packet.

An ideal four-port optical device couples two fields quantized along the directions of the input ports (labeled by 1 and 2) obeying

$$[\hat{a}_1(\omega), \hat{a}_2^\dagger(\omega')] = 0 \ . \tag{16}$$

The simultaneous excitation of a single-photon wave packet in each field can be described by the operator product

$$\begin{aligned} \hat{K}^\dagger(\epsilon_1,\epsilon_2) &\equiv \hat{A}_1^\dagger(\epsilon_1)\hat{A}_2^\dagger(\epsilon_2) \\ &= \int_0^\infty \int_0^\infty \epsilon_1(\omega)\epsilon_2(\omega')\hat{a}_1^\dagger(\omega)\hat{a}_2^\dagger(\omega')d\omega\, d\omega' \ , \end{aligned} \tag{17}$$

provided that the two wave packets are created independently. However, this assumption is too restrictive to account for wave packets that originate together from a common source.

A more general formalism incorporates the joint complex amplitude $\zeta(\omega,\omega')$,

$$\hat{K}^\dagger(\zeta) \equiv \int_0^\infty \int_0^\infty \zeta(\omega,\omega')\hat{a}_1^\dagger(\omega)\hat{a}_2^\dagger(\omega')d\omega\, d\omega' \ , \tag{18}$$

which describes the simultaneous excitation of the fields. This joint wave-packet operator obeys the commutator

$$[\hat{K}(\zeta), \hat{K}^\dagger(\zeta)] = \hat{I} + \hat{N}_1 + \hat{N}_2 \ , \tag{19}$$

as long as the amplitude $\zeta(\omega,\omega')$ is normalized via

$$\int_0^\infty \int_0^\infty |\zeta(\omega,\omega')|^2 d\omega\, d\omega' = 1 \ . \tag{20}$$

The operators $\hat{N}_1$ and $\hat{N}_2$ are normally ordered

$$\hat{N}_j \equiv \int_0^\infty \int_0^\infty \xi_j(\omega,\omega')\hat{a}_j^\dagger(\omega)\hat{a}_j(\omega')d\omega\, d\omega' \ , \quad j=1,2 \tag{21a}$$

$$\xi_1(\omega,\omega') \equiv \int_0^\infty \zeta(\omega,\Omega)\zeta^*(\omega',\Omega)d\Omega \ , \tag{21b}$$

$$\xi_2(\omega,\omega') \equiv \int_0^\infty \zeta(\Omega,\omega)\zeta^*(\Omega,\omega')d\Omega \ , \tag{21c}$$

and do not contribute to expectations in the vacuum.

A joint single-photon wave-packet state is created according to

$$\begin{aligned} |1_1,1_2;\zeta\rangle &\equiv \hat{K}^\dagger(\zeta)|0,0\rangle \\ &= \int_0^\infty \int_0^\infty \zeta(\omega,\omega')|1_\omega\rangle|1_{2\omega'}\rangle d\omega\, d\omega' \ , \end{aligned} \tag{22}$$

such that the joint probability $P(\omega,\omega')d\omega\, d\omega'$ of exciting a photon frequency between ω and $\omega+d\omega$ in the first field and another of frequency between ω' and $\omega'+d\omega'$ in

the second field is given by

$$P(\omega,\omega')d\omega\,d\omega' \equiv |\langle 1_{1\omega}|\langle 1_{2\omega'}|1_1,1_2;\zeta\rangle|^2 d\omega\,d\omega' = |\zeta(\omega,\omega')|^2 d\omega\,d\omega' \ . \tag{23}$$

To obtain the coherence properties of this state, we first note, in analogy with Eq. (7), that the product of the two positive-frequency portions of the field operators, at the respective times t' and t, can be represented by

$$\hat{E}_2^{(+)}(t')\hat{E}_1^{(+)}(t) = (2\pi)^{-1} \times \int_0^\infty \int_0^\infty \hat{a}_1(\omega)\hat{a}_2(\omega') \times e^{-i(\omega t+\omega' t')} d\omega\,d\omega' \Longleftrightarrow V(t,t')\hat{K}(\zeta) \ , \tag{24}$$

where $V(t,t')$ is the joint temporal profile of the wave packet,

$$V(t,t') \equiv (2\pi)^{-1} \int_0^\infty \int_0^\infty \zeta(\omega,\omega') e^{-i(\omega t+\omega' t')} d\omega\,d\omega' \ . \tag{25}$$

The Glauber second-order correlation function for the product of the positive-frequency parts of the fields at times t' and t, with the adjoint product at times $t+\tau$ and $t'+\tau'$,[10] follows from Eqs. (19), (22), and (24),

$$G^{(2)}(t,t',\tau,\tau') \equiv \mathrm{Tr}[\hat{\rho}\hat{E}_1^{(-)}(t+\tau)\hat{E}_2^{(-)}(t'+\tau') \times \hat{E}_2^{(+)}(t')\hat{E}_1^{(+)}(t)] = V^*(t+\tau,t'+\tau')V(t,t') \ , \tag{26}$$

given the density operator $\hat{\rho}=|1_1,1_2;\zeta\rangle\langle 1_1,1_2;\zeta|$. The normalized, time-averaged second-order correlation function is provided by Eqs. (23)–(26),

$$\gamma(\tau,\tau') \equiv \frac{\int_{-\infty}^\infty \int_{-\infty}^\infty G^{(2)}(t,t',\tau,\tau')dt\,dt'}{\int_{-\infty}^\infty \int_{-\infty}^\infty G^{(2)}(t,t',0,0)dt\,dt'} = \int_0^\infty \int_0^\infty P(\omega,\omega')e^{i(\omega\tau+\omega'\tau')}d\omega\,d\omega' \ . \tag{27}$$

This is the characteristic function of the joint probability density $P(\omega,\omega')$, in analogy with that of Eq. (10) for a single-photon wave packet. Coherence times for the joint single-photon wave packet can now be defined

$$t_\pm \equiv \pi^{-1/2} \int_{-\infty}^\infty |\gamma(\tau,\pm\tau)|^2 d\tau \ , \tag{28}$$

such as to accentuate the joint nature of this wave-packet mode.

To illustrate the above, we consider a joint single-photon wave packet described by the complex amplitude

$$\zeta(\omega,\omega') = (2\pi\sigma^2)^{-1/2}(1-\eta^2)^{-1/4}\exp[-Q(\omega,\omega')/2] \times \exp(-i\omega t_1)\exp(-i\omega' t_2) \ , \tag{29a}$$

$$Q(\omega,\omega') \equiv \frac{(\omega-\omega_1)^2+(\omega'-\omega_2)^2-2\eta(\omega-\omega_1)(\omega'-\omega_2)}{2\sigma^2(1-\eta^2)} \ , \tag{29b}$$

and possessing the joint Gaussian probability density[13]

$$P(\omega,\omega') = (2\pi\sigma^2)^{-1}(1-\eta^2)^{-1/2}\exp[-Q(\omega,\omega')] \ , \tag{30}$$

where (ω_1,ω_2) and (t_1,t_2) are the center frequencies and time shifts associated with the constituent Gaussian wave packets of spectral width σ, and the parameter η reflects their degree of correlation.

When $\eta=0$, this joint wave packet factorizes into two independent single-photon Gaussian wave packets, each with an amplitude in the form of Eq. (12). On the other hand, when $\eta=\mp 1$, the Gaussian wave packets have complete spectral anticorrelation and correlation, respectively, since the frequencies ω and ω' are then constrained by the relationships[13]

$$\omega \pm \omega' = \omega_1 \pm \omega_2 \ . \tag{31}$$

Although $P(\omega,\omega')$ is strictly not a probability density when $\eta=\mp 1$, these limits are nevertheless valid as long as they are taken after the calculation of statistical quantities. In the limit $\eta\to -1$, this joint single-photon wave packet then provides a suitable model for each pair of photons emitted from a parametric down-converter, which is governed by sum-frequency conservation.[14]

The characteristic function of the joint Gaussian probability density is well known. With the narrow-band approximation ($\sigma \ll \omega_1,\omega_2$), the correlation function represented in Eq. (27) is given by[13]

$$\gamma(\tau,\tau') = \exp[-\sigma^2(\tau^2+\tau'^2+2\eta\tau\tau')/2] \times \exp(i\omega_1\tau)\exp(i\omega_2\tau') \ , \tag{32}$$

yielding, via Eq. (28), the joint coherence times

$$t_\pm = \frac{1}{\sigma[2(1\pm\eta)]^{1/2}} \ . \tag{33}$$

These joint coherence times depend on the inverse bandwidth σ of the photon wave packets, *as well as* on their degree η of spectral correlation. Consequently, for complete spectral anticorrelation or correlation ($\eta=-1$ and $+1$), t_+ and t_- become infinite, respectively, whatever the value of the finite coherence time $t_c=1/\sigma$ [Eq. (15)]. We will show in Sec. III that the coincidence detection of joint single-photon wave packets is governed by the joint coherence times, and therefore reflects the entangled nature of two photons emerging from a common source.

III. FOURTH-ORDER INTERFERENCE OF JOINT SINGLE-PHOTON WAVE PACKETS

Fourth-order interference properties can be measured with a pair of photodetectors working in coincidence. The response of these detectors is given by correlation functions in the form of Eq. (26), evaluated at zero lag times.[10,11]

Consider a joint single-photon wave packet presented to a lossless optical system with two input ports, such as a beam splitter or an interferometer (see Fig. 1). The coincidence rates at input ports 1 and 2 are then given by

$$G_{11}^{(2)}(t,t') \equiv \mathrm{Tr}[\hat{\rho}\hat{E}_1^{(-)}(t)\hat{E}_1^{(-)}(t')\hat{E}_1^{(+)}(t')\hat{E}_1^{(+)}(t)] = 0 \ , \tag{34a}$$

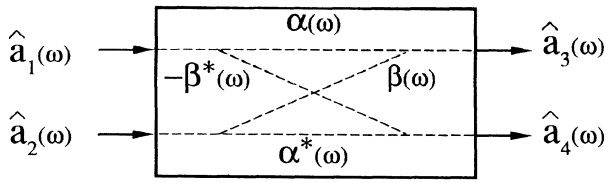

FIG. 1. A four-port lossless optical device can be represented by a unitary transformation of two fields at each frequency ω. The transformation is governed by the complex transmission coefficient $\alpha(\omega)$ and reflection coefficient $\beta(\omega)$, which are related by $|\alpha(\omega)|^2+|\beta(\omega)|^2=1$.

$$G_{22}^{(2)}(t,t')\equiv \mathrm{Tr}[\hat{\rho}\hat{E}_2^{(-)}(t)\hat{E}_2^{(-)}(t')\hat{E}_2^{(+)}(t')\hat{E}_2^{(+)}(t)] =0 , \tag{34b}$$

$$G_{12}^{(2)}(t,t')\equiv \mathrm{Tr}[\hat{\rho}\hat{E}_1^{(-)}(t)\hat{E}_2^{(-)}(t')\hat{E}_2^{(+)}(t')\hat{E}_1^{(+)}(t)] =|V(t,t')|^2 , \tag{34c}$$

where $\hat{\rho}=|1_1,1_2;\zeta\rangle\langle 1_1,1_2;\zeta|$, and $V(t,t')$ is the temporal profile of the joint single-photon wave packet, as indicated in Eq. (25). This result ensures that coincidence counts are not registered at either input port alone, because the input photon pair is divided between them.

A lossless optical system effects an SU(2) unitary transformation on the input fields, as shown schematically in Fig. 1. The fields at the output ports 3 and 4 are given by[15–17]

$$\hat{E}_j^{(+)}(t)=(2\pi)^{-1/2}\int_0^\infty \hat{a}_j(\omega)e^{-i\omega t}d\omega, \quad j=3,4 , \tag{35a}$$

$$\begin{bmatrix}\hat{a}_3(\omega)\\ \hat{a}_4(\omega)\end{bmatrix}=\begin{bmatrix}\alpha(\omega) & \beta(\omega)\\ -\beta^*(\omega) & \alpha^*(\omega)\end{bmatrix}\begin{bmatrix}\hat{a}_1(\omega)\\ \hat{a}_2(\omega)\end{bmatrix} , \tag{35b}$$

where $\alpha(\omega)$ and $\beta(\omega)$ are complex field transmission and reflection coefficients specific to the device under consideration, and are related by

$$|\alpha(\omega)|^2+|\beta(\omega)|^2=1 . \tag{36}$$

The coincidence rates at the output ports are then found to be

$$G_{33}^{(2)}(t,t')\equiv \mathrm{Tr}[\hat{\rho}\hat{E}_3^{(-)}(t)\hat{E}_3^{(-)}(t')\hat{E}_3^{(+)}(t')\hat{E}_3^{(+)}(t)] =|V_a(t,t')|^2+|V_a(t',t)|^2 +2\,\mathrm{Re}[V_a^*(t,t')V_a(t',t)] , \tag{37a}$$

$$G_{44}^{(2)}(t,t')\equiv \mathrm{Tr}[\hat{\rho}\hat{E}_4^{(-)}(t)\hat{E}_4^{(-)}(t')\hat{E}_4^{(+)}(t')\hat{E}_4^{(+)}(t)] =|V_b(t,t')|^2+|V_b(t',t)|^2 +2\,\mathrm{Re}[V_b^*(t,t')V_b(t',t)] , \tag{37b}$$

$$G_{34}^{(2)}(t,t')\equiv \mathrm{Tr}[\hat{\rho}\hat{E}_3^{(-)}(t)\hat{E}_4^{(-)}(t')\hat{E}_4^{(+)}(t')\hat{E}_3^{(+)}(t)] =|V_c(t,t')|^2+|V_d(t',t)|^2 -2\,\mathrm{Re}[V_c^*(t,t')V_d(t',t)] , \tag{37c}$$

where Re denotes the real part, and we have defined

$$V_a(t,t')\equiv(2\pi)^{-1}\int_0^\infty\int_0^\infty \alpha(\omega)\beta(\omega')\zeta(\omega,\omega') \times e^{-i(\omega t+\omega' t')}d\omega\,d\omega' , \tag{38a}$$

$$V_b(t,t')\equiv(2\pi)^{-1}\int_0^\infty\int_0^\infty \beta^*(\omega)\alpha^*(\omega')\zeta(\omega,\omega') \times e^{-i(\omega t+\omega' t')}d\omega\,d\omega' , \tag{38b}$$

$$V_c(t,t')\equiv(2\pi)^{-1}\int_0^\infty\int_0^\infty \alpha(\omega)\alpha^*(\omega')\zeta(\omega,\omega') \times e^{-i(\omega t+\omega' t')}d\omega\,d\omega' , \tag{38c}$$

$$V_d(t,t')\equiv(2\pi)^{-1}\int_0^\infty\int_0^\infty \beta^*(\omega)\beta(\omega')\zeta(\omega,\omega') \times e^{-i(\omega t+\omega' t')}d\omega\,d\omega' . \tag{38d}$$

These functions represent transformations of the input wave packet's temporal profile [Eq. (25)] by the device. Coincidence counts can now be observed not only between the two ouput ports, but also at either output port alone.

Practical coincidence detectors register integrations of Eq. (37) over a coincidence counting time for the duration of the experiment. When these times are very much larger than the temporal spread of the photons after path-length time shifts are imposed by the optical system, Eq. (37) is twice integrated from $(-\infty,\infty)$ to obtain the coincidence probabilities

$$P_{\mathrm{out}}(2,0)=\tfrac{1}{2}\int_{-\infty}^\infty\int_{-\infty}^\infty G_{33}^{(2)}(t,t')dt\,dt' =\int_0^\infty\int_0^\infty|\alpha(\omega)|^2|\beta(\omega')|^2P(\omega,\omega')d\omega\,d\omega'+\int_0^\infty\int_0^\infty[\alpha(\omega)\alpha^*(\omega')\beta^*(\omega)\beta(\omega')]\zeta(\omega,\omega')\zeta^*(\omega',\omega)d\omega\,d\omega' , \tag{39}$$

$$P_{\mathrm{out}}(0,2)=\tfrac{1}{2}\int_{-\infty}^\infty\int_{-\infty}^\infty G_{44}^{(2)}(t,t')dt\,dt' =\int_0^\infty\int_0^\infty|\beta(\omega)|^2|\alpha(\omega')|^2P(\omega,\omega')d\omega\,d\omega'+\int_0^\infty\int_0^\infty[\alpha(\omega)\alpha^*(\omega')\beta^*(\omega)\beta(\omega')]\zeta(\omega,\omega')\zeta^*(\omega',\omega)d\omega\,d\omega' , \tag{40}$$

$$P_{\mathrm{out}}(1,1)=\int_{-\infty}^\infty\int_{-\infty}^\infty G_{34}^{(2)}(t,t')dt\,dt' =\int_0^\infty\int_0^\infty[|\alpha(\omega)|^2|\alpha(\omega')|^2+|\beta(\omega)|^2|\beta(\omega')|^2]P(\omega,\omega')d\omega\,d\omega' -2\int_0^\infty\int_0^\infty[\alpha(\omega)\alpha^*(\omega')\beta^*(\omega)\beta(\omega')]\zeta(\omega,\omega')\zeta^*(\omega',\omega)d\omega\,d\omega' . \tag{41}$$

The factor of $\frac{1}{2}$ in Eqs. (39) and (40) removes the doubling that accompanies the second-order correlation function of the field in a two-photon state. The first integral on the right-hand side of each of these probabilities describes the appropriate transmission and reflection combinations that take the photons from input to output, spectrally averaged over the joint probability density $P(\omega,\omega')$ of the input wave packet. For instance, in Eq. (41) coincidences between the output ports occur when the input photons are either both transmitted or both reflected. The last term in Eq. (41) expresses interference between these two possibilities in an integral containing the phase-sensitive overlap of the joint amplitudes $\zeta(\omega,\omega')$ and $\zeta^*(\omega',\omega)$.

The above results are applicable to any lossless optical device with two input ports, such as a beam splitter or a Mach-Zehnder interferometer. We illustrate the theory by considering these two devices in turn.

A. Beam splitter

The lossless beam splitter shown in Fig. 2 is represented by Eq. (35) with the transmission and reflection coefficients[15–17]

$$\alpha(\omega)=T^{1/2}(\omega),\quad \beta(\omega)=R^{1/2}(\omega)\ , \tag{42}$$

where $T(\omega)$ and $R(\omega)=1-T(\omega)$ are the transmittance and reflectance of a dispersive beam splitter. Without loss of generality, we have assumed that no phase shift is imparted to the input beams by the beam splitter. In practice, beam splitters are often nondispersive over the spectral range of interest, in which case

$$T(\omega)=T,\quad R(\omega)=R=1-T\ . \tag{43}$$

Substituting this result in Eqs. (39)–(41), we obtain

$$P_{\rm out}(2,0)=P_{\rm out}(0,2)=TR\,[1+\Phi(0,0)]\ , \tag{44a}$$

$$P_{\rm out}(1,1)=T^2+R^2-2TR\,\Phi(0,0)\ , \tag{44b}$$

where $\Phi(0,0)$ is a special case of the general integral

$$\Phi(\tau,\tau')\equiv\int_0^\infty\int_0^\infty \zeta(\omega,\omega')\zeta^*(\omega',\omega)e^{i(\omega\tau+\omega'\tau')}d\omega\,d\omega'\ . \tag{45}$$

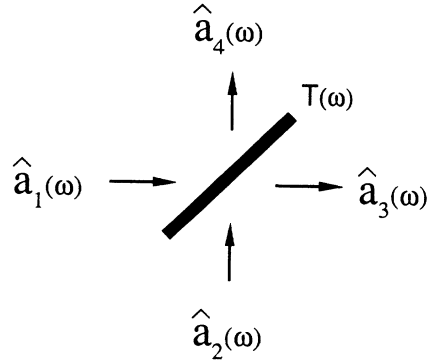

FIG. 2. The lossless beam splitter is an optical device governed by its transmittance $T(\omega)$.

This integral, which is evaluated in Appendix A for a wave packet with a joint Gaussian spectrum, will be used in the study of the Mach-Zehnder interferometer. The fact that $\tau=\tau'=0$ in Eq. (44) reflects the fact that the beam splitter was assumed not to impart any phase shifts to the fields at its inputs. However, $\Phi(0,0)$ does account for any path-length time difference the photons may have at the input of the device, which is contained in the amplitude $\zeta(\omega,\omega')$.

The transmission and reflection terms in Eq. (44) that do not depend on $\Phi(0,0)$ are consistent with the binomial statistics that result from independent Bernoulli trials for two distinguishable classical particles.[5] The terms containing $\Phi(0,0)$ depend explicitly on the joint spectral character of the input state and represent quantum interference that arises from our inability to determine how the photons are distributed into the output ports of the beam splitter. As a result, there is generally an increased probability of observing both photons at either output port, and a corresponding decrease in the probability of observing one photon at each output port. When the photons are totally indistinguishable, $P_{\rm out}(2,0)=P_{\rm out}(0,2)=2TR$ while $P_{\rm out}(1,1)=(T-R)^2$.[4,6,17]

Substituting Eq. (A7) with $\tau=\tau'=0$ into Eq. (44b), we obtain a coincidence probability given by

$$P_{\rm out}(1,1)=T^2+R^2-2TR\exp(-\omega_d^2t_-^2/2)\times\exp(-\tau_{\rm in}^2/2t_-^2)\ , \tag{46}$$

where t_- is the joint coherence time given by Eq. (33), ω_d is the difference $|\omega_1-\omega_2|$ between the center frequencies of the photons' Gaussian spectral distributions, and $\tau_{\rm in}$ is the path-length time difference of the photons in entering the beam splitter. It is clear from Eq. (46) that the photons will not exhibit fourth-order interference if they are distinguishable by color $[\exp(-\omega_d^2t_-^2/2)\ll 1]$, or if they are temporally distinguishable $[\exp(-\tau_{\rm in}^2/2t_-^2)\ll 1]$.

We evaluate Eq. (46) for different degrees of spectral correlation η given a 50-50 beam splitter ($T=R=\frac{1}{2}$). For completely anticorrelated and uncorrelated photons ($\eta=-1$ and 0, respectively), we find

$$P_{\rm out}(1,1)=\begin{cases}\frac{1}{2}[1-\exp(-\omega_d^2t_c^2/8)\exp(-2\tau_{\rm in}^2/t_c^2)], & \eta=-1 \quad (47a)\\ \frac{1}{2}[1-\exp(-\omega_d^2t_c^2/4)\exp(-\tau_{\rm in}^2/t_c^2)], & \eta=0, \quad (47b)\end{cases}$$

where $t_c=1/\sigma$ is the coherence time of the individual photons. These coincidence probabilities approach zero when the photons have the same center frequency ($\omega_d=0$) and when they suffer the same time delay to the input ports of the beam splitter ($\tau_{\rm in}=0$), as shown in Fig. 3(a). As the two photons become increasingly separated in time at the input, the coincidence probability between the output ports rises and eventually saturates to a constant level (classical-particle behavior) when $\tau_{\rm in}$ greatly exceeds t_c. At this point they are temporally distinguish-

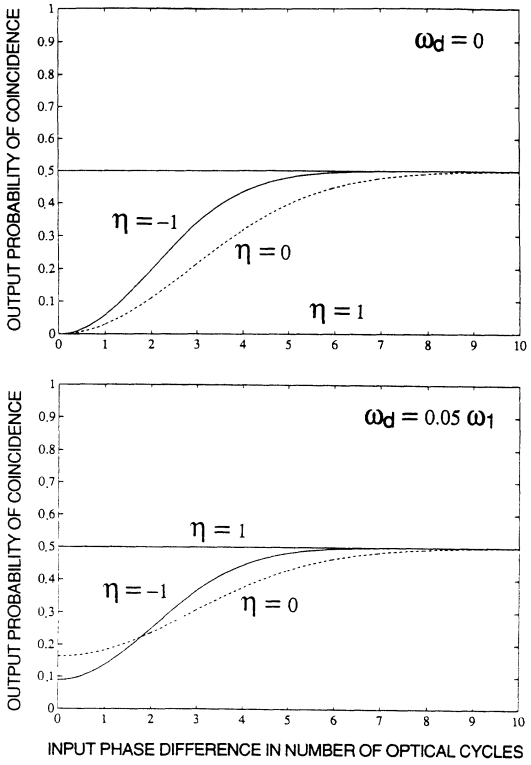

FIG. 3. The coincidence probability $P_{\text{out}}(1,1)$ at the output ports of a 50-50 ($T=\frac{1}{2}$) lossless nondispersive beam splitter is shown when a wave packet described by a joint Gaussian probability density is incident on it, with one photon impinging on each of its ports [Eqs. (47) and (48)]. The result is plotted vs the input path-length difference $|\tau_{\text{in}}|$ of the two photons, expressed in terms of the number of optical cycles of the center frequency of the first photon's spectral distribution ($\omega_1|\tau_{\text{in}}|/2\pi$). (a) The center frequency of the second photon is the same as that of the first ($\omega_2=\omega_1$ so that $\omega_d=|\omega_1-\omega_2|=0$), and the spectral width σ of both photons was chosen to be $\sigma=\omega_1/8\pi$. For completely anticorrelated and uncorrelated photons ($\eta=-1$ and 0, respectively) the coincidence probability is zero at $\tau_{\text{in}}=0$ and rises to a constant value of $\frac{1}{2}$ when the photons are temporally well separated at the inputs. However, for completely correlated ($\eta=1$) photons, this probability is zero for all $|\tau_{\text{in}}|$. (b) The center frequenccy of the second photon $\omega_2=0.95\omega_1$, so that $\omega_d=0.05\omega_1$. Again, $\sigma=\omega_1/8\pi$. The 5% spectral mismatch significantly reduces the cancellation of the coincidence probability for $\eta=-1$ and 0. For completely correlated photons ($\eta=1$), no reduction is observed for all time differences.

able and no longer manifest fourth-order interference.

When $\omega_d\neq 0$, completely anticorrelated photons produce a larger reduction in the coincidence probability than uncorrelated photons, but the effect occurs within a shorter range of τ_{in} [see Fig. 3(b)]. The fourth-order interference of completely anticorrelated photons at a single beam splitter has been verified experimentally by Hong, Ou, and Mandel,[4] and by Rarity and Tapster,[6] with twin photons from a parametric down-converter. Both groups permitted a center-frequency difference no greater than the spectral width of the photons ($\omega_d\approx\sigma\approx 10^{13}$ rad/sec), corresponding to a wavelength difference of the order of a few nanometers ($\lambda_d\approx 5$ nm).

Completely correlated photons ($\eta=1$) behave like monochromatic ones ($\sigma=0$) at the beam splitter because the joint coherence time t_- becomes infinite [see Eq. (33)]. Thus using Eq. (46) with $T=R=\frac{1}{2}$ we obtain

$$P_{\text{out}}(1,1)=\begin{cases}0, & \omega_d=0, \quad \eta=1\\ \frac{1}{2}, & \omega_d\neq 0, \quad \eta=1\end{cases}. \tag{48}$$

As shown in Fig. 3, the coincidence probability can only be reduced (in fact, canceled) when $\omega_d=0$, and it is then independent of τ_{in}.

B. Mach-Zehnder interferometer

A lossless Mach-Zehnder interferometer (MZI) is illustrated schematically in Fig. 4. The first beam splitter of transmittance $T_1(\omega)$ apportions the input light into the interferometer. A path-length difference ΔL may be introduced between the arms of the interferometer, prior to the recombination of the two optical beams at the second beam splitter of transmittance $T_2(\omega)$. As shown in Appendix B, the MZI is represented by Eq. (35) with

$$\begin{aligned}\alpha(\omega)&=T_1^{1/2}(\omega)R_2^{1/2}(\omega)\exp(i\omega\tau_{\text{MZ}}/2)\\&\quad+R_1^{1/2}(\omega)T_2^{1/2}(\omega)\exp(-i\omega\tau_{\text{MZ}}/2),\\ \beta(\omega)&=R_1^{1/2}(\omega)R_2^{1/2}(\omega)\exp(i\omega\tau_{\text{MZ}}/2)\\&\quad-T_1^{1/2}(\omega)T_2^{1/2}(\omega)\exp(-i\omega\tau_{\text{MZ}}/2),\end{aligned} \tag{49}$$

where $R_1(\omega)=1-T_1(\omega)$ and $R_2(\omega)=1-T_2(\omega)$ are the reflectances of the two lossless beam splitters, and $\tau_{\text{MZ}}\equiv\Delta L/c$. We assume that the input beams maintain perfect spatial alignment through the device. The coincidence probabilities at the output of the MZI have a greater range of behavior than those at the output of the beam splitter because of the additional degree of freedom provided by the variable time delay τ_{MZ}.

To calculate the coincidence probability between the output ports, we assume that the beam splitters of the MZI are nondispersive, as in Eq. (43). Substituting Eq. (49) into Eq. (41) yields

$$\begin{aligned}P_{\text{out}}(1,1)&=T_{\text{MZ}}(\tau_{\text{MZ}},0)T_{\text{MZ}}(0,\tau_{\text{MZ}})+R_{\text{MZ}}(\tau_{\text{MZ}},0)R_{\text{MZ}}(0,\tau_{\text{MZ}})\\&\quad+4T_1R_1T_2R_2\text{Re}[\gamma(\tau_{\text{MZ}},\tau_{\text{MZ}})-\gamma(\tau_{MZ},0)\gamma(0,\tau_{\text{MZ}})+\gamma(\tau_{\text{MZ}},-\tau_{\text{MZ}})-\gamma(\tau_{\text{MZ}},0)\gamma(0,-\tau_{\text{MZ}})]\\&\quad-2(T_2-R_2)^2T_1R_1\Phi(0,0)-4(T_2-R_2)(T_1R_1T_2R_2)^{1/2}\text{Re}[T_1\Phi(\tau_{\text{MZ}},0)-R_1\Phi(0,\tau_{\text{MZ}})]\\&\quad-2T_2R_2T_1^2\Phi(\tau_{\text{MZ}},-\tau_{\text{MZ}})-2T_2R_2R_1^2\Phi(-\tau_{\text{MZ}},\tau_{\text{MZ}})+4T_1R_1T_2R_2\text{Re}[\Phi(\tau_{\text{MZ}},\tau_{MZ})],\end{aligned} \tag{50}$$

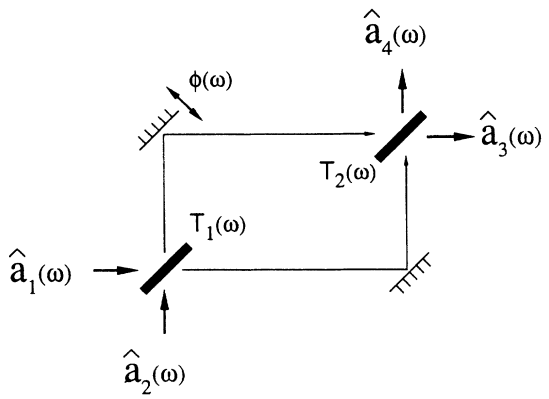

FIG. 4. The lossless Mach-Zehnder interferometer (MZI) has beam splitters with transmittances $T_1(\omega)$ and $T_2(\omega)$ and a path-length phase shift $\phi(\omega)=\omega\tau_{MZ}$, where $\tau_{MZ}\equiv\Delta L/c$ depends on the path-length difference ΔL between the two arms of the device. The MZI is a special case of the transformation shown in Fig. 1.

where $\gamma(\tau,\tau')$ and $\Phi(\tau,\tau')$ are given by Eqs. (27) and (45), respectively, and the functions $T_{MZ}(\,)$ and $R_{MZ}(\,)$ are defined as

$$T_{MZ}(\tau_{MZ},0)\equiv T_1R_2+R_1T_2 +2(T_1R_1T_2R_2)^{1/2}\mathrm{Re}[\gamma(\tau_{MZ},0)]\ , \quad (51a)$$

$$R_{MZ}(\tau_{MZ},0)\equiv T_1T_2+R_1R_2 -2(T_1R_1T_2R_2)^{1/2}\mathrm{Re}[\gamma(\tau_{MZ},0)]\ , \quad (51b)$$

$$T_{MZ}(0,\tau_{MZ})\equiv T_1R_2+R_1T_2 +2(T_1R_1T_2R_2)^{1/2}\mathrm{Re}[\gamma(0,\tau_{MZ})]\ , \quad (51c)$$

$$R_{MZ}(0,\tau_{MZ})\equiv T_1T_2+R_1R_2 -2(T_1R_1T_2R_2)^{1/2}\mathrm{Re}[\gamma(0,\tau_{MZ})]\ . \quad (51d)$$

The quantities in Eq. (51) represent the global transmittance and reflectance for each photon of the joint wave packet passing through the interferometer. The first two terms of these functions outline the two paths the photon could take at the device if it were to behave as a classical distinguishable particle. Consider, for example, the first of these equations: a particle at the first input port of the MZI (port 1) can be transmitted to the first ouput port (port 3) either by being transmitted at the first beam splitter and reflected at the second (T_1R_2), or by being reflected at the first beam splitter and transmitted at the second (R_1T_2). The additional term represents the usual second-order interference resulting from the uncertainty of which of these two paths is followed by the photon.[3]

The first two terms in Eq. (50) therefore represent products of second-order interference patterns that would give rise to coincidences between the output ports if the photons were to behave independently at the input. However, for jointly distributed photons, the correlation function $\gamma(\tau,\tau')$ need not factorize into the product $\gamma(\tau,0)\gamma(0,\tau')$ of the marginal correlation functions, so that the joint behavior in the coincidence probability is accounted for in the third term. The function $\Phi(\tau,\tau')$, which appears in the remainder of the equation, provides fourth-order interference effects that depend on the indistinguishability of the photons. It is sensitive to the relative time delay of the photons at the input to the interferometer $|\tau_{in}|$, as we have seen in the case of the beam splitter [Eq. (44)], as well as to the path-length time difference imparted by the interferometer $|\tau_{MZ}|$.

If the MZI has 50-50 beam splitters ($T_1=R_1=T_2=R_2=\frac{1}{2}$), the coincidence probability between the output ports simplifies considerably,

$$P_{out}(1,1)=\tfrac{1}{2}+\tfrac{1}{4}\mathrm{Re}[\gamma(\tau_{MZ},\tau_{MZ}) +\gamma(\tau_{MZ},-\tau_{MZ})+\Phi(\tau_{MZ},\tau_{MZ})] -\tfrac{1}{8}\Phi(\tau_{MZ},-\tau_{MZ})-\tfrac{1}{8}\Phi(-\tau_{MZ},\tau_{MZ})\ , \quad (52)$$

exhibiting only joint functions. As an illustration, we consider the joint single-photon wave packet described by Eq. (29). Substituting Eqs. (32) and (A7) into Eq. (52), and employing Eq. (33) together with the definitions in Eqs. (A6) and (A8), we obtain

$$P_{out}(1,1)=\tfrac{1}{2}+\tfrac{1}{4}[\exp(-\tau_{MZ}^2/2t_+^2)\cos(\omega_s\tau_{MZ})+\exp(-\tau_{MZ}^2/2t_-^2)\cos(\omega_d\tau_{MZ})] +\tfrac{1}{4}\exp(-\omega_d^2t_-^2/2)\exp(-\tau_{in}^2/2t_-^2)[\exp(-\tau_{MZ}^2/2t_+^2)\cos(\omega_s\tau_{MZ})-\exp(-\tau_{MZ}^2/2t_-^2)\cosh(\tau_{MZ}\tau_{in}/t_-^2)]\ . \quad (53)$$

This coincidence probability depends on both of the joint coherence times t_+ and t_-, and on the sum frequency ω_s, unlike that between the output ports of a single beam splitter given in Eq. (46).

When the photons are distinguishable by color [$\exp(-\omega_d^2t_-^2/2)\ll 1$], or by nonoverlap in time [$\exp(-\tau_{in}^2/2t_-^2)\ll 1$], the last term in Eq. (53) vanishes, in which case

$$P_{out}(1,1)=\tfrac{1}{2}+\tfrac{1}{4}[\exp(-\tau_{MZ}^2/2t_+^2)\cos(\omega_s\tau_{MZ}) +\exp(-\tau_{MZ}^2/2t_-^2)\cos(\omega_d\tau_{MZ})]\ . \quad (54)$$

In the former case, the correlation function $\gamma(\tau,\tau')$ results in beats in the coincidence probability for interferometer path-length differences within the coherence time t_c, as shown in Fig. 5.

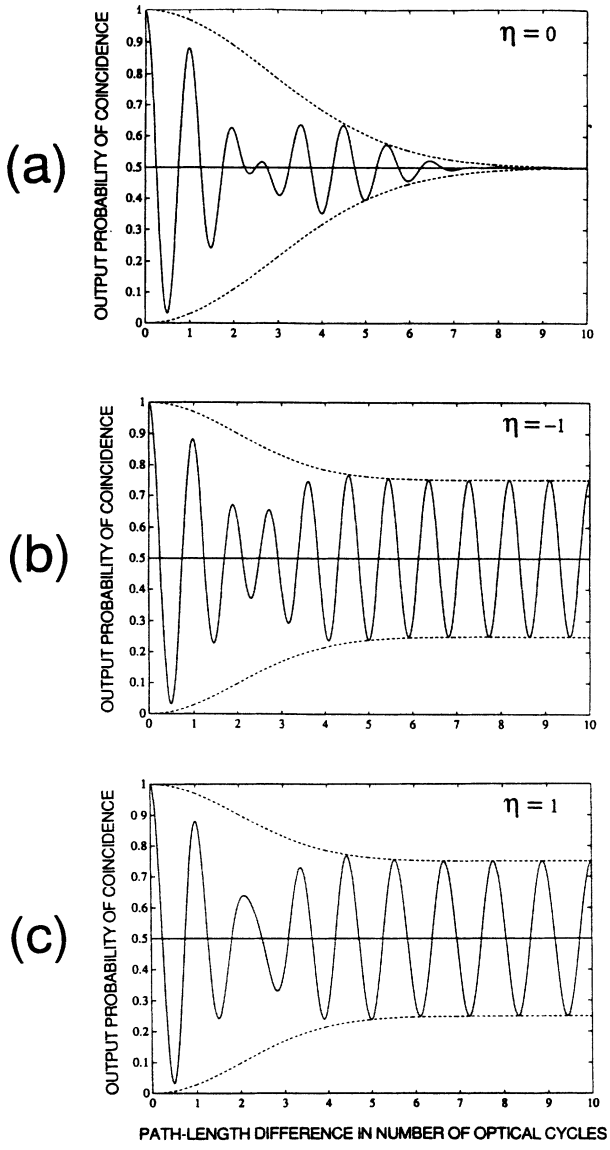

FIG. 5. The coincidence probability $P_{\text{out}}(1,1)$ at the output ports of a lossless Mach-Zehnder interferometer with 50-50 nondispersive beam splitters is shown when a wave packet described by a joint Gaussian probability density is incident on it, with one photon impinging on each of its ports [Eqs. (55) and (56)]. The result is plotted vs the path-length difference $|\tau_{\text{MZ}}|$ between the arms of the interferometer, expressed in terms of the number of optical cycles of the center frequency of the first photon's spectral distribution ($\omega_1|\tau_{\text{MZ}}|/2\pi$). In the example shown here, the center frequency of the second photon is $\omega_2=0.1\omega_1$ so that $\omega_d=|\omega_1-\omega_2|=0.9\omega_1$, the spectral width of both photons is $\sigma=\omega_1/8\pi$, and the relative time delay of the photons at the input to the interferometer is arbitrary. (a) For uncorrelated photons ($\eta=0$), the coincidence probability exhibits oscillations at the sum ($\omega_s=\omega_1+\omega_2=1.1\omega_1$) and difference ($\omega_d=0.9\omega_1$) frequencies that decay as the interferometer's path-length difference is increased from zero. (b) For completely anticorrelated photons ($\eta=-1$), the sum-frequency oscillations are independent of $|\tau_{\text{MZ}}|$. (c) For completely correlated photons ($\eta=1$) the difference-frequency oscillations are independent of $|\tau_{\text{MZ}}|$. The probability of coincidence is never canceled in all cases.

Using Eq. (33), we find that for uncorrelated photons ($\eta=0$) the joint coherence times t_+ and t_- are equal ($t_+=t_-=t_c/2^{1/2}$), giving rise to a balanced superposition of sum- and difference-frequency oscillations,

$$P_{\text{out}}(1,1)=\tfrac{1}{2}+\tfrac{1}{4}\exp(-\tau_{\text{MZ}}^2/t_c^2)\times[\cos(\omega_s\tau_{\text{MZ}})+\cos(\omega_d\tau_{\text{MZ}})]\ ,\qquad \eta=0\ . \tag{55}$$

Increasing the path-length time-difference τ_{MZ} in the interferometer from zero past the second-order coherence time t_c causes the oscillations to damp out, as shown in Fig. 5(a).

However, the joint coherence times governing the sum- and difference-frequency oscillations can be quite different if the photons are completely anticorrelated or correlated. In the former case ($\eta=-1$) these times are given by $t_\pm=(\infty, t_c/2)$, so the sum-frequency component in Eq. (54) does not decay with increasing path-length difference, whereas in the latter case ($\eta=1$) the situation is reversed $t_\pm=(t_c/2,\infty)$, and the difference-frequency component does not damp out:

$$P_{\text{out}}(1,1)=\begin{cases}\tfrac{1}{2}+\tfrac{1}{4}[\cos(\omega_s\tau_{\text{MZ}})+\exp(-2\tau_{\text{MZ}}^2/t_c^2)\cos(\omega_d\tau_{\text{MZ}})]\ , & \eta=-1 \quad (56a)\\ \tfrac{1}{2}+\tfrac{1}{4}[\exp(-2\tau_{\text{MZ}}^2/t_c^2)\cos(\omega_s\tau_{\text{MZ}})+\cos(\omega_d\tau_{\text{MZ}})], & \eta=1\ . \quad (56b)\end{cases}$$

The behavior of these two coincidence probabilities are shown in Figs. 5(b) and 5(c), respectively. In both cases it settles down to a constant visibility

$$[P_{\text{out}}^{\max}(1,1)-P_{\text{out}}^{\min}(1,1)]/[P_{\text{out}}^{\max}(1,1)+P_{\text{out}}^{\min}(1,1)]=50\%$$

at large values of the path-length difference.

When the photons arrive at the input with a large time delay between them [$\exp(-\tau_{\text{in}}^2/2t_-^2)\ll 1$], but are indistinguishable by color ($\omega_d=0$), Eq. (53) reduces to

$$P_{\text{out}}(1,1)=\tfrac{1}{2}+\tfrac{1}{4}[\exp(-\tau_{\text{MZ}}^2/2t_+^2)\cos(\omega_s\tau_{\text{MZ}})+\exp(-\tau_{\text{MZ}}^2/2t_-^2)]\ . \tag{57}$$

The sum-frequency oscillations (which are now at twice the center frequency of the input photons) remain, whereas the difference-frequency oscillations are now at *dc*. This formula does not apply to completely correlated photons, since it is only valid for $\exp(-\tau_{\text{in}}^2/2t_-^2)\ll 1$, and $t_-\to\infty$. The behavior is quite different for the two remaining types of spectral correlation,

$$P_{\text{out}}(1,1)=\begin{cases}\tfrac{1}{2}+\tfrac{1}{4}\exp(-\tau_{\text{MZ}}^2/t_c^2)[\cos(\omega_s\tau_{\text{MZ}})+1], & \eta=0 \quad (58a)\\ \tfrac{1}{2}+\tfrac{1}{4}[\cos(\omega_s\tau_{\text{MZ}})+\exp(-2\tau_{\text{MZ}}^2/t_c^2)], & \eta=-1. \quad (58b)\end{cases}$$

For uncorrelated photons, the coincidence probability exhibits decaying sum-frequency oscillations with increasing interferometer path-length difference above the constant level $\frac{1}{2}$, as shown in Fig. 6(a). On the other hand, completely anticorrelated photons produce undamped sum-frequency oscillations about a level that decays from $\frac{3}{4}$ for small path-length differences to $\frac{1}{2}$ at large path-length differences. The visibility increases from 33% to 50% as the path-length difference is increased. Figure 6(b) illustrates this behavior.

The color and time distinguishability of the photons in the above two regimes of MZI operation forbids a total cancellation of the coincidence probability, as seen in Figs. 5 and 6. As in the case of the single 50-50 beam splitter shown in Fig. 3, complete quenching is permitted only when the photons have the same center frequency ($\omega_d=0$) and arrive together at the interferometer ($\tau_{\rm in}=0$). In this case Eq. (53) reduces to

$$P_{\rm out}(1,1)=\tfrac{1}{2}[1+\exp(-\tau_{\rm MZ}^2/2t_+^2)\cos(\omega_s\tau_{\rm MZ})] \ . \quad (59)$$

For uncorrelated and completely correlated photons, the coincidence probability is given by

$$P_{\rm out}(1,1)=\begin{cases}\tfrac{1}{2}[1+\exp(-\tau_{\rm MZ}^2/t_c^2)\cos(\omega_s\tau_{\rm MZ})] \ , & \\ \qquad\qquad \eta=0 & \text{(60a)}\\ \tfrac{1}{2}[1+\exp(-2\tau_{\rm MZ}^2/t_c^2)\cos(\omega_s\tau_{\rm MZ})], & \\ \qquad\qquad \eta=1 \ , & \text{(60b)}\end{cases}$$

respectively. As shown in Figs. 7(a) and 7(c), $P_{\rm out}(1,1)$ oscillates symmetrically about the value $\frac{1}{2}$ and decays as

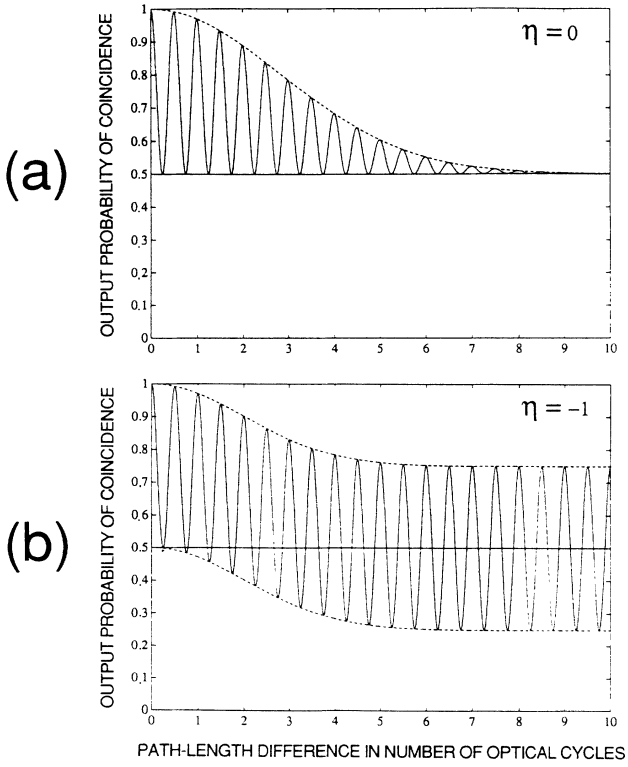

FIG. 6. Same as Fig. 5, except that $\omega_d=0$ and $\exp[-\sigma^2\tau_{\rm in}^2(1-\eta)]\ll 1$ [Eq. (58)]. Spectrally correlated ($\eta=1$) photons cannot satisfy this condition. (a) For uncorrelated photons ($\eta=0$), the coincidence probability exhibits decaying sum-frequency oscillations (at $\omega_s=2\omega_1$) about the constant level $\frac{1}{2}$ as the interferometer's path-length difference is increased. (b) For completely anticorrelated photons ($\eta=-1$) these oscillations are undamped, but the level about which they appear gradually decreases. In both cases the probability of coincidence never reaches zero.

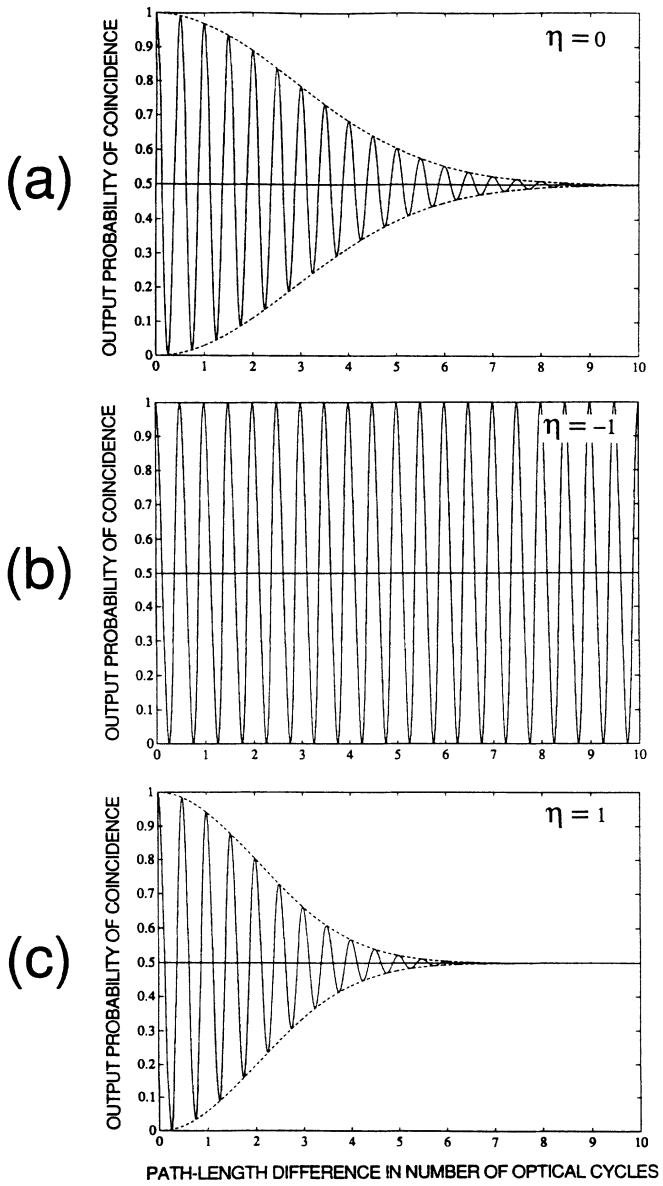

FIG. 7. Same as Fig. 5, but the photons have equal center frequencies ($\omega_d=0$) and are coincident in time at the input to the interferometer ($\tau_{\rm in}=0$) [Eqs. (60) and (61)]. (a) For uncorrelated photons ($\eta=0$) and (c) for completely correlated photons ($\eta=1$), the sum-frequency oscillations are damped out as the path-length difference of the device is increased, while (b) for completely anticorrelated photons ($\eta=-1$) these oscillations have 100% visibility and manifest a periodic cancellation of the coincidence probability for values of $|\tau_{\rm MZ}|$ exceeding the coherence time $t_c=1/\sigma$ of either photon.

the path-length time difference of the interferometer is increased from zero.

However, completely anticorrelated photons obey

$$P_{\text{out}}(1,1)=\tfrac{1}{2}[1+\cos(\omega_s\tau_{\text{MZ}})],\quad \eta=-1 \tag{61}$$

which provides a periodic cancellation of the coincidence probability for arbitrarily large values of the path-length difference, as can be seen in Fig. 7(b). $P_{\text{out}}(1,1)$ therefore exhibits oscillations at the sum frequency $\omega_s=2\omega_1$, with a constant visibility of 100%. Since Eq. (61) is independent of the photons' bandwidth, the same result can be obtained directly from a single-mode theory for the interference of two, two-photon probability amplitudes.[7,18]

IV. DISCUSSION

We have obtained the coincidence probabilities at the output of an arbitrary four-port lossless optical device when a joint single-photon wave packet is incident at its inputs, one photon at each port. We have explicitly evaluated the coincidence probability between the output ports when a wave packet described by a joint Gaussian spectral distribution is incident on a beam splitter [Eq. (46)] and on a Mach-Zehnder interferometer [Eq. (53)]. In both cases this coincidence probability is governed by joint coherence times that depend on the spectral relationship of the input photons. For complete spectral correlation or anticorrelation the joint coherence times can be infinite, even if the photons have a finite coherence time.

The parametric down-converter is a source of spectrally anticorrelated photon pairs. Experiments with down-converted photons at a single Mach-Zehnder interferometer have confirmed the existence of fourth-order oscillations in the coincidence probability at the pump frequency, with $\approx 60\%$ visibility, for interferometer path-length time differences exceeding the coherence time of either photon.[19] Similar interference effects have been observed (but with visibilities $<50\%$) in experiments where each photon of the down-converted pair was sent to separate Michelson interferometers prior to coincidence detection.[20,21] Fourth-order interference effects like these are unequivocal demonstrations of the entangled nature of joint single-photon wave packets.

ACKNOWLEDGMENTS

This work was supported by the Joint Services Electronics Program through the Columbia Radiation Laboratory. We are indebted to J. G. Rarity and P. R. Tapster of the Royal Signals and Radar Establishment in Malvern, England, for directing our attention to the properties of photon pairs from parametric down-conversion. We are grateful to T. Larchuk and F. Singer for useful discussions.

APPENDIX A: INTEGRAL OF THE JOINT-GAUSSIAN WAVE-PACKET AMPLITUDE

We calculate the integral

$$\Phi(\tau,\tau')=\int_0^\infty\int_0^\infty \zeta(\omega,\omega')\zeta^*(\omega',\omega) \times\exp[i(\omega\tau+\omega'\tau')]d\omega\,d\omega' , \tag{A1}$$

where $\zeta(\omega,\omega')$ is the joint Gaussian complex amplitude in Eq. (29), which is given by

$$\zeta(\omega,\omega')=(2\pi\sigma^2)^{-1/2}(1-\eta^2)^{-1/4}\exp[-Q(\omega,\omega')/2] \times\exp[-i(\omega t_1+\omega' t_2)] , \tag{A2}$$

$$Q(\omega,\omega')\equiv\frac{(\omega-\omega_1)^2+(\omega'-\omega_2)^2-2\eta(\omega-\omega_1)(\omega'-\omega_2)}{2\sigma^2(1-\eta^2)} .$$

Substituting Eq. (A2) in Eq. (A1), we obtain

$$\Phi(\tau,\tau')=(2\pi\sigma^2)^{-1}(1-\eta^2)^{-1/2} \times\int_0^\infty\int_0^\infty\exp\{-[Q(\omega,\omega')+Q(\omega',\omega)]/2\} \times\exp[i\omega(\tau-\tau_{\text{in}})] \times\exp[i\omega'(\tau'+\tau_{\text{in}})]d\omega\,d\omega' , \tag{A3}$$

where we have defined the input time lag

$$\tau_{\text{in}}\equiv(t_1-t_2) . \tag{A4}$$

Expanding the function Q and collecting terms, we can rewrite Eq. (A3) as

$$\Phi(\tau,\tau')=\gamma(\tau,\tau')\exp[-\tau_{\text{in}}(\tau_{\text{in}}+\tau'-\tau)/2t_-^2] \times\exp[i\omega_d(i\omega_d t_-^2+\tau'-\tau)/2] , \tag{A5}$$

where ω_d is the absolute value of the difference in the center frequencies of the two jointly distributed Gaussian wave packets,

$$\omega_d\equiv|\omega_1-\omega_2| , \tag{A6}$$

and $\gamma(\tau,\tau')$ is the second-order correlation function of Eq. (32). Substituting $\gamma(\tau,\tau')$ and employing Eqs. (15) and (33), we finally obtain

$$\Phi(\tau,\tau')=\exp[-\omega_d^2 t_-^2/2]\exp[-\tau_{\text{in}}^2/2t_-^2] \times\exp[-(\tau+\tau')^2/2t_c^2]\exp[-\tau_{\text{in}}(\tau'-\tau)/2t^2] \times\exp[\tau\tau'/2t_-^2]\exp[i\omega_s(\tau+\tau')/2] . \tag{A7}$$

This function exhibits exponential scaling factors, a decaying Gaussian envelope in τ and τ', and oscillations at the sum frequency

$$\omega_s\equiv\omega_1+\omega_2 . \tag{A8}$$

APPENDIX B: FIELD TRANSFORMATIONS OF THE MACH-ZEHNDER INTERFEROMETER

The transmission and reflection coefficients of the lossless Mach-Zehnder interferometer (Fig. 4) can be obtained by using the following SU(2) unitary transforma-

tions of the input boson operators $\hat{a}_1(\omega)$ and $\hat{a}_2(\omega)$ at the angular frequency ω:[15–17]

$$\begin{bmatrix} T^{1/2}(\omega) & R^{1/2}(\omega) \\ -R^{1/2}(\omega) & T^{1/2}(\omega) \end{bmatrix} \begin{bmatrix} \hat{a}_1(\omega) \\ \hat{a}_2(\omega) \end{bmatrix}, \tag{B1}$$

$$\begin{bmatrix} \exp[i\phi(\omega)/2] & 0 \\ 0 & \exp[-i\phi(\omega)/2] \end{bmatrix} \begin{bmatrix} \hat{a}_1(\omega) \\ \hat{a}_2(\omega) \end{bmatrix}. \tag{B2}$$

Equation (B1) represents the field transformation of a lossless beam splitter with transmittance $T(\omega)$ and reflectance $R(\omega)=1-T(\omega)$, whereas Eq. (B2) represents the effects of a phase shift $\phi(\omega)$. The Mach-Zehnder interferometer may be constructed by cascading a beam splitter of transmittance $T_1(\omega)$, a linear path-length-difference phase shift $\phi(\omega)=\omega\tau_{\mathrm{MZ}}$, where $\tau_{\mathrm{MZ}}\equiv\Delta L/c$, a mirror reflection, and another beam splitter of transmittance $T_2(\omega)$. Using the corresponding matrices in succession, we find that this interferometer is represented by the field transformation matrix

$$\begin{aligned} &\begin{bmatrix} T_2^{1/2}(\omega) & R_2^{1/2}(\omega) \\ -R_2^{1/2}(\omega) & T_2^{1/2}(\omega) \end{bmatrix} \begin{bmatrix} 0 & -1 \\ 1 & 0 \end{bmatrix} \\ &\quad\times \begin{bmatrix} \exp(i\omega\tau_{\mathrm{MZ}}/2) & 0 \\ 0 & \exp(-i\omega\tau_{\mathrm{MZ}}/2) \end{bmatrix} \\ &\quad\times \begin{bmatrix} T_1^{1/2}(\omega) & R_1^{1/2}(\omega) \\ -R_1^{1/2}(\omega) & T_1^{1/2}(\omega) \end{bmatrix} \\ &\quad= \begin{bmatrix} \alpha(\omega) & \beta(\omega) \\ -\beta^*(\omega) & \alpha^*(\omega) \end{bmatrix}, \end{aligned} \tag{B3}$$

provided

$$\begin{aligned} \alpha(\omega) &= T_1^{1/2}(\omega)R_2^{1/2}(\omega)\exp(i\omega\tau_{\mathrm{MZ}}/2) \\ &\quad + R_1^{1/2}(\omega)T_2^{1/2}(\omega)\exp(-i\omega\tau_{\mathrm{MZ}}/2), \\ \beta(\omega) &= R_1^{1/2}(\omega)R_2^{1/2}(\omega)\exp(i\omega\tau_{\mathrm{MZ}}/2) \\ &\quad - T_1^{1/2}(\omega)T_2^{1/2}(\omega)\exp(-i\omega\tau_{\mathrm{MZ}}/2). \end{aligned} \tag{B4}$$

[1] C. A. Kocher and E. D. Commins, Phys. Rev. Lett. **18**, 575 (1967).

[2] D. C. Burnham and D. L. Weinberg, Phys. Rev. Lett. **25**, 84 (1970).

[3] P. Grangier, G. Roger and A. Aspect, Europhys. Lett. **1**, 173 (1986); A. Aspect, P. Grangier, and G. Roger, J. Opt. (Paris) **20**, 119 (1989).

[4] C. K. Hong, Z. Y. Ou, and L. Mandel, Phys. Rev. Lett. **59**, 2044 (1987).

[5] J. Brendel, S. Schütrumpf, R. Lange, W. Martienssen, and M. O. Scully, Europhys. Lett. **5**, 223 (1988); R. Lange, J. Brendel, E. Mohler, and W. Martienssen, *ibid.* **5**, 619 (1988).

[6] J. G.. Rarity and P. R. Tapster, J. Opt. Soc. Am. B **6**, 1221 (1989).

[7] E. Mohler, J. Brendel, R. Lange, and W. Martienssen, Europhys. Lett. **8**, 511 (1989).

[8] U. M. Titulaer and R. J. Glauber, Phys. Rev. **145**, 1041 (1966).

[9] H. Fearn and R. Loudon, Opt. Commun. **64**, 485 (1987); H. Fearn and R. Loudon, J. Opt. Soc. Am. B **6**, 917 (1989); see also R. Loudon, in *Coherence and Quantum Optics VI,* edited by J. H. Eberly, L. Mandel, and E. Wolf (Plenum, New York, in press).

[10] R. J. Glauber, Phys. Rev. **130**, 2529 (1963).

[11] R. J. Glauber, in *Quantum Optics,* edited by S. M. Kay and A. Maitland (Academic, London, 1970).

[12] L. Mandel and E. Wolf, Proc. Phys. Soc. (London) **80**, 894 (1962).

[13] J. B. Thomas, *An Introduction to Applied Probability and Random Processes* (Wiley, New York, 1971).

[14] R. Ghosh, C. K. Hong, Z. Y. Ou, and L. Mandel, Phys. Rev. A **34**, 3962 (1986).

[15] B. L. Schumaker, Phys. Rep. **135**, 317 (1986).

[16] B. Yurke, S. L. McCall, and J. R. Klauder, Phys. Rev. A **33**, 4033 (1986).

[17] R. A. Campos, B. E. A. Saleh, and M. C. Teich, Phys. Rev. A **40**, 1371 (1989).

[18] R. Ghosh and L. Mandel, Phys. Rev. Lett. **59**, 1903 (1987).

[19] J. G. Rarity, P. R. Tapster, E. Jakeman, T. Larchuk, R. A. Campos, M. C. Teich, and B. E. A. Saleh, Phys. Rev. Lett. **65**, 1348 (1990).

[20] Z. Y. Ou, X. Y. Zou, L. J. Wang, and L. Mandel, Phys. Rev. Lett. **65**, 321 (1990).

[21] P. G. Kwiat, W. A. Vareka, C. K. Hong, H. Nathel, and R. Y. Chiao, Phys. Rev. A **41**, 2910 (1990).